Turbulence generation during the head-on collision of Alfvénic wave packets

O. Pezzi,[1] F. Malara,[1] S. Servidio,[1] F. Valentini,[1] T. N. Parashar,[2] W. H. Matthaeus,[2] and P. Veltri[1]
[1]*Dipartimento di Fisica, Università della Calabria, 87036 Rende (CS), Italy*
[2]*Department of Physics and Astronomy, University of Delaware, Newark Delaware 19716, USA*
(Received 13 March 2017; published 7 August 2017)

The description of the Moffatt and Parker problem recently revisited by O. Pezzi *et al.* [Astrophys. J. **834**, 166 (2017)] is here extended by analyzing the features of the turbulence produced by the interaction of two colliding Alfvénic wave packets in a kinetic plasma. Although the approach based on the presence of linear modes features is still helpful in characterizing some low-energy fluctuations, other signatures, which go beyond the pure linear modes analysis, are recovered, such as the significant weakening of clear dispersion relations and the production of zero frequency fluctuations.

DOI: 10.1103/PhysRevE.96.023201

I. INTRODUCTION

The main mechanism of turbulence is the nonlinear coupling among fluctuations, which transfers energy to different spatial scales, thus generating the turbulence spectrum (e.g., Ref. [1]). In the ideal incompressible magnetohydrodynamics (MHD), where fields are often expressed in terms of the Elsässer variables $\mathbf{z}^{\pm} = \mathbf{u} \pm \mathbf{b}/(4\pi\rho)^{1/2}$ ($\mathbf{u}$, $\mathbf{b}$, and ρ being the velocity, magnetic field, and density, respectively) [2], a peculiar aspect is that nonlinear couplings can take place only between $\delta\mathbf{z}^{+}$ and $\delta\mathbf{z}^{-}$ fluctuations. In this context, Moffatt [3] and Parker [4] considered the problem of the collision of two large-amplitude spatially localized Alfvén wave packets, oppositely propagating along the background magnetic field $\mathbf{B}_0$, which can be seen as $\mathbf{z}^{+}$ and $\mathbf{z}^{-}$ perturbations. Wave packets propagate undistorted until overlapping, when they start being modified by nonlinear interactions. Then wave packets eventually separate and propagate once again undisturbed without further interactions. The interaction between oppositely propagating Alfvénic packets has been considered as the "building block" of nonlinear phenomena taking place in incompressible MHD turbulence [5–10]. The relevance of this phenomenon is also due to the fact that Alfvénic perturbations represent the main component of fluctuations in weakly compressible natural plasmas, as directly measured in the fast streams of solar wind [11,12] and inferred in the solar corona by remote sensing observations [13–16].

However, the incompressible approximation is often not fully adequate, since it neglects, obviously compressions, but also dispersion and kinetic effects. Indeed, although many intervals of solar wind are highly Alfvénic [17,18], small density variations and a small parallel magnetic field variance are found, as in the often-quoted 5:4:1 variance ratio [11]. Moreover, at smaller scales near the ion inertial scale, kinetic properties are observed, such as spectral steepening [12,19], dispersive wave effects [20–22], temperature anisotropy, beams, and other distortions of the proton velocity distribution function (VDF) [23–30]. These considerations place the problem of the collision of Alfvén wave packets in a much more complex framework.

In two previous papers [31,32] (hereafter Papers I and II), we revisited the collision of two large-amplitude Alfvénic wave packets by means of compressible MHD, Hall MHD, and hybrid Vlasov-Maxwell (HVM) numerical simulations. Results showed a dynamics more complex than that envisaged by Moffatt and Parker in the ideal incompressible MHD case: (1) the complexity of structures produced by nonlinear interactions makes it difficult to determine whether wave packets are fully separated after their collision, (2) the time behavior of several integral quantities is different from that expected in the ideal incompressible MHD case, and (3) a tendency has been found to build up nearly isotropic spectra, with slope about $\sim -5/3$, in the plane almost perpendicular to $\mathbf{B}_0$.

A similar problem, concerning the interaction of nonlocalized moderate-amplitude Alfvén waves at spatial scales comparable with the ion inertial length, has been approached within the weak turbulence framework [33]; moreover gyro-kinetic simulations [34] and laboratory experiments [35–37] have been performed in a similar context. This approach is often based on the assumption of small-amplitude fluctuations and describes turbulence in terms of weakly nonlinear couplings among waves, each belonging to a well-defined propagating mode and maintaining its own distinctive properties (e.g., dispersion relation, etc). The theory of weak turbulence in plasmas has been widely studied within MHD [8,38], including dispersive effects [39], and also for high-frequency waves [40–42]. Moreover, within this framework, properties concerning the Landau damping of a kinetic Alfvén wave (KAW) or its absorption in an inhomogeneous plasma have been investigated in detail [43–45]. Strong and weak turbulence theories may be viewed as complementary [46,47], and there is a debate on the applicability of a "wave approach" to describe, for instance, turbulence in the solar wind [48–54]. In the present paper we intend to give further contributions to these fundamental issues.

In the large-amplitude packets collision considered here, the ratio between the nonlinear time $\tau_{nl} = \Delta/u$ and characteristic wave-packet collision time $\tau_{\mathrm{coll}} = \Delta/V$ is about $1/2$ (where Δ, u and V are, respectively, the wave packet width, the perturbation amplitude and the in-plane propagation speed). This indicates that wave packets are significantly modified by nonlinear couplings also in a single collision. The purpose of the present paper is to give some insights concerning the kind of interactions that occur between the packets and to analyze, in particular, the fluctuations generated by the collision in terms of properties associated either with linear modes, or with turbulence. Signatures of localized waves have

been also recovered in a fully turbulent scenario driven by the Kelvin-Helmholtz instability [55]. Here we show that wavelike activity, characterized by the presence of linear plasma mode features, diminishes in favor of turbulence even if one starts with Alfvénic wave packets. In particular, we point out that some fluctuations generated by nonlinear interactions display polarization and correlation properties typical of linear modes. However, after the collision, the frequency-wave-number branches appear significantly broadened and tend to build up quasi stationary structures.

II. NUMERICAL APPROACH AND INITIAL CONDITION

Here we numerically solve the hybrid Vlasov-Maxwell (HVM) system of equations for a quasineutral plasma composed of kinetic, collisionless protons, and fluid Maxwellian electrons [24]. The phase space configuration is $2.5D$–$3V$, which means that all the vector components are retained, but they depend only on two spatial coordinates $\mathbf{x} = (x,y)$. Dimensionless HVM equations are

$$\partial_t f + \mathbf{v}\cdot\nabla f + (\mathbf{E} + \mathbf{v}\times\mathbf{B})\cdot\nabla_{\mathbf{v}} f = 0, \tag{1}$$

$$\mathbf{E} - d_e^2\Delta\mathbf{E} = -\mathbf{u_e}\times\mathbf{B} - \frac{\nabla P_e}{n} + \frac{d_e^2}{n}\{\nabla\cdot\Pi + n\mathbf{u}\times\mathbf{B} + \nabla\cdot[n(\mathbf{u}\mathbf{u} - \mathbf{u_e}\mathbf{u_e})]\}, \tag{2}$$

$$\partial_t\mathbf{B} = -\nabla\times\mathbf{E}, \quad \nabla\times\mathbf{B} = \mathbf{j}, \tag{3}$$

where $f = f(\mathbf{x},\mathbf{v},t)$ is the proton distribution function, $\mathbf{E}(\mathbf{x},t)$ is the electric field, $\mathbf{B}(\mathbf{x},t) = \mathbf{B_0} + \mathbf{b}(\mathbf{x},t)$ is the total magnetic field, and $\mathbf{j} = \nabla\times\mathbf{B}$ is the total current density. Proton density $n(\mathbf{x},t)$ and mean velocity $\mathbf{u}(\mathbf{x},t)$ are obtained as velocity moments of the proton distribution function f. Moreover, a quasineutrality condition ($n = n_p = n_e$) and an isothermal equation of state for the electron pressure P_e are assumed. To prevent numerical instabilities electron inertia effects have been considered in Ohm's law using an electron-to-ion mass ratio $m_e/m_p = d_e^2 = 0.01$ (being d_e the electron skin depth), while no external resistivity has been imposed. Since the scale associated with d_e is almost at the limit of the accessible scales of our simulation, we can reasonably expect that the present value of mass ratio does not influence the results presented here, which occur on scales much larger than d_e. In Eqs. (1)–(3) time, velocities, lengths, and masses are scaled to the inverse ion cyclotron frequency Ω_{cp}^{-1}, to the Alfvén speed c_A, to the proton skin depth $d_p = c/\omega_{pp} = c_A/\Omega_{cp}$ (being c the light speed and ω_{pp} the proton plasma frequency) and to the proton mass m_p, respectively. For the sake of simplicity, all quantities will be scaled as prescribed above. Note that, since here we focus on the HVM simulation, the normalizations are different from the ones adopted in Papers I and II. A detailed description of the numerical method employed to solve Eqs. (1)–(3) can be found in Ref. [24].

Equations (1)–(3) are integrated in a double periodic box $D(x,y) = [0,L_x]\times[0,L_y]$, being $L_x = 256$ and $L_y = 64$, which has been discretized with $(N_x,N_y) = (1024,256)$ points. Each direction of the velocity space is discretized in the region $v_i = [-5v_{th,p},5v_{th,p}]$ with $N_{v_i} = 51$ mesh points ($i = x,y,z$), where $\beta_p = 2v_{th,p}^2/c_A^2 = 0.5$ and $v_{th,p}^2 = k_B T_p/m_p$ is the proton thermal speed. Boundary conditions in the velocity domain assume $f = 0$ for $|v_i| > 5v_{th,p}$.

The background magnetic field $\mathbf{B_0}$ is mainly perpendicular to the x-y plane: $\mathbf{B_0} = B_0(\sin\vartheta,0,\cos\vartheta)$, where $\vartheta = \cos^{-1}[(\mathbf{B_0}\cdot\hat{\mathbf{z}})/B_0] = 6^\circ$ and $B_0 = |\mathbf{B_0}| = 1$ in code units. At $t = 0$, the proton VDF is a nondrifting Maxwellian at each spatial point. Then, magnetic $\mathbf{b}$ and mean velocity $\mathbf{u}$ perturbations are introduced, while no density perturbations are imposed. As described in Paper I, initial fluctuations consist of two quasi-Alfvénic wave packets with opposite velocity-magnetic field correlation, separated along x. Since $B_{0,x} \neq 0$, wave packets counterpropagate and collide after a time about $\tau = 600$. The intensity of the perturbation is $\langle b\rangle_{\rm rms}/B_0 = 0.2$ and the Mach number is $M = \langle u\rangle_{\rm rms}/v_{th,p} = 0.4$. A detailed discussion of the properties of the initial conditions can be found in Paper I.

III. SIMULATION RESULTS

The evolution of the two wave packets can be easily appreciated in Fig. 1, where the shaded surface of the current density $j_z(x,y,t)$ is reported. The horizontal plane corresponds to x-y plane, while the temporal evolution is given by the vertical direction. The two wave packets start their motion by approaching each other; then, around $t = \tau$, they collide, producing complex current structures. During the collision wave packets interact and change shape, by forming smaller-scale fluctuations. As reported in Paper I, magnetic energy spectra tend to become isotropic in the plane, indicating the presence of quasiperpendicular nonlinear couplings, leading to a slope close to $-5/3$. The conservation of the Vlasov

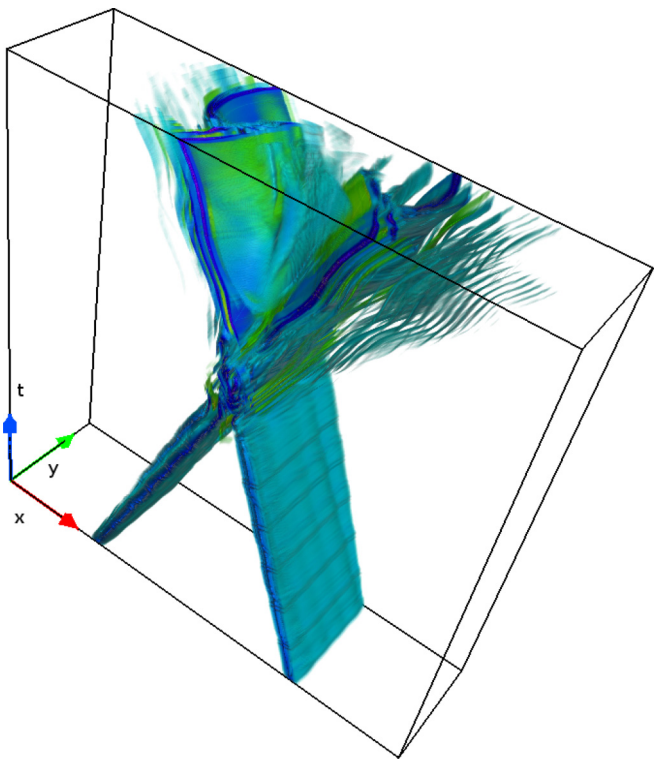

FIG. 1. Space-time representation of Alfvénic packets collision by means of the iso-surfaces of the current density $j_z(x,y,t)$.

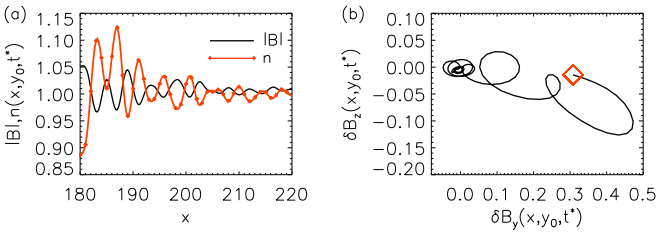

FIG. 2. (a) Shape of $|\mathbf{B}|$ (solid black) and n (dot-solid red) as a function of x in the region $x = [180,220]$, for $y = y_0 = 12$ and $t = t^* = 1020$. (b) Hodogram of $\delta B_z(x,y_0,t^*)$ as a function of $\delta B_y(x,y_0,t^*)$ for $x = [180,220]$, $y = y_0 = 12$ and $t = t^* = 1020$. The red square indicates the initial x point $x = 180$.

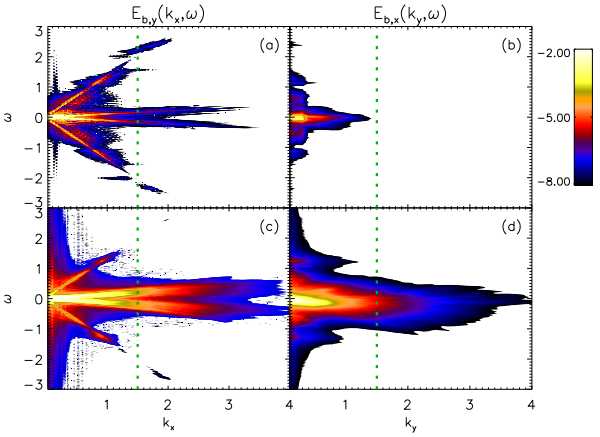

FIG. 3. Contour plots of $E_{b,y}(k_x,\omega) = \langle E_b(\mathbf{k},\omega)\rangle_{k_y}$ (left) and $E_{b,x}(k_y,\omega) = \langle E_b(\mathbf{k},\omega)\rangle_{k_x}$ (right) in region I (before collision, top) and in region II (after collision, bottom). The green dashed lines indicate the wave number $k^* = 1.5$, at which the cuts reported in Fig. 4 have been performed.

invariants in the present simulation is well respected (see Ref. [56] for a detailed discussion). Indeed, the mass, total energy, and entropy are respectively conserved up to 0.1%, 0.5%, and 1%.

Here we focus on the description of some significant features which are recovered after the collision. In particular, small-amplitude ripples, which propagate almost purely along x, appear in front of each wave packet. Moreover, at the center of the spatial domain, some vortical current sheet structures are also present and can be clearly appreciated looking at the temporal evolution of $j_z(x,y,t)$, which is showed in the Supplemental Material [57].

To understand the physical mechanism driving the production of these secondary small-amplitude ripples, whose wavelength is $\simeq$5.9, Fig. 2(a) reports the evolution of $|\mathbf{B}|(x,y_0,t^*)$ (solid black) and $n(x,y_0,t^*)$ (dot-solid red) as a function of x, zoomed in the region $x = [180,220]$ (where these disturbances are present) for $y = y_0 = 12$ and at $t = t^* = 1020$. Density n and $|\mathbf{B}|$ fluctuations are anticorrelated, this being typical of kinetic Alfvén waves and slow magnetosonic modes [22,58,59]. In order to differentiate between the two waves branches, we study their polarization by making the hodogram of two magnetic field components [58]. Figure 2(b) reports the hodogram of $\delta B_z(x,y_0,t^*)$ as a function of $\delta B_y(x,y_0,t^*)$, in the region $x = [180,220]$ for $y = y_0 = 12$ and at $t = t^* = 1020$. The red square in Fig. 2(b) reports the initial point $x = 180$. The hodogram shows a clockwise rotation with increasing x that is compatible only with KAWs or fast magnetosonic waves. We computed the propagation speed of these fluctuations, finding that this, too, is compatible with the KAWs' propagation speed. Therefore, based on these three signatures (correlations, polarization, and propagation speed), we conclude that these small-amplitude fluctuations are compatible with KAWs. The presence of these fluctuations is a byproduct of the wave packets interaction: since initial disturbances are mainly Alfvénic, the energy is transferred along the Alfvén wave branch, thus generating these KAW-like ripples.

A description of the system solely in terms of linear plasma mode features is, however, restrictive, and the small-amplitude KAWs are just one element of a more complex scenario. Indeed, since $\tau_{nl}/\tau_{\rm coll} < 1$, features typical of a turbulent regime may be also reached. To point out that the picture is actually more complex, we performed the following analysis. We selected two temporal windows of duration $T \simeq 300$ (about 600 time steps), before (I) and after (II) the wave packets collision. In both windows, the magnetic energy $E_b(\mathbf{x},t) \simeq \delta\mathbf{B}^2$ is quite stationary. This allows us to implement a full spatio-temporal Fourier transform of $E_b(\mathbf{x},t)$ to obtain $E_b(\mathbf{k},\omega)$, thus providing the magnetic energy distribution in the spectral space ω-$\mathbf{k}$. We should remark that the ω resolution in our case ($\Delta\omega = 2\pi/T \approx 2\times10^{-2}$) is significantly finer than the value recovered through spacecraft measurements [51–54].

Figure 3 reports the contour plots of $E_{b,y}(k_x,\omega) = \langle E_b(\mathbf{k},\omega)\rangle_{k_y}$ (left) and $E_{b,x}(k_y,\omega) = \langle E_b(\mathbf{k},\omega)\rangle_{k_x}$ (right) in region I (top) and II (bottom). Before the interaction, the energy $E_{b,y}(k_x,\omega)$ is recovered mostly at relatively larger scales and is distributed in two branches of waves: Alfvénic (smaller phase speed) and fast magnetosonic (larger phase speed). Note that, since the background magnetic field is quasiperpendicular to the propagation plane, the Alfvén speed projected onto the x-y plane is much smaller compared to the fast magnetosonic phase speed. The coexistence of different waves branches before the main interaction of the two wave packets confirms that our initial perturbations are not purely Alfvénic packets but also include some compressive fluctuations. Some Bernstein fluctuations are also present along the fast waves branch at high frequencies. The energy $E_{b,x}(k_y,\omega)$ is significantly peaked around $\omega \approx 0$ at larger wavelength.

The magnetic energy distribution changes after the wave packets collision. First, smaller spatial scales are populated, as can be easily appreciated in Figs. 3(c)–3(d), due to the nonlinear couplings which transfer energy towards larger wave number. However, the energy distribution is significantly spread in the ω-k space and does not rigidly follow the standard dispersion relations: a conelike region is populated along the k_x direction, while a wide blob, peaked at $\omega = 0$, is covered in the k_y direction. Hence, the presence of dispersion relations is significantly weakened after a single collision thus suggesting that turbulence is fundamental for describing the interaction of colliding wave packets. We expect that the dynamics would be even closer to a fully developed turbulent scenario if wave packets could interact several times or for a longer time period.

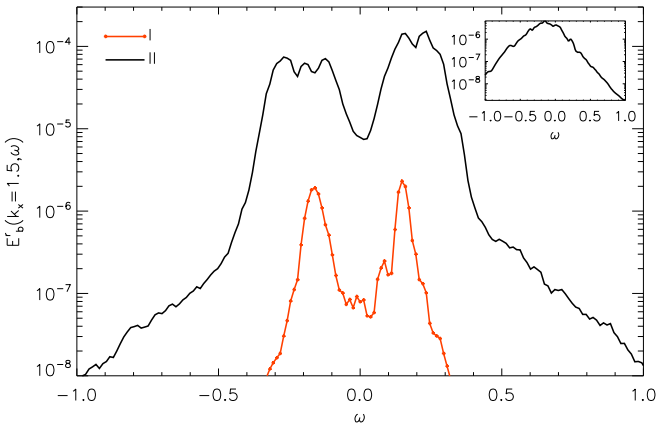

FIG. 4. Plot of $E_{b,y}(k_x = 1.5,\omega)$ as a function of ω in the region I (solid black) and II (dot-solid red). The small inset plots $E_{b,x}(k_y = 1.5,\omega)$ as a function of ω in the region II.

Figure 4 reports the profile of $E_{b,y}(k_x = k^*,\omega)$ as a function of ω and at a given $k_x = k^* = 1.5$, while the inset of Fig. 4 reports $E_{b,x}(k_y = k^*,\omega)$ as a function of ω and at a given $k_y = k^* = 1.5$. The range of ω in Fig. 4 has been opportunely chosen to focus on Alfvénic fluctuations. Dot-solid red and solid black lines in Fig. 4 refer to the temporal windows before (I) and after (II) the wave packets collision, respectively. Figure 4 is essentially a cut of Figs. 3 at a given wave number, indicated with a green dashed line. Clearly, the growth of the amplitude of $E_{b,x}(k_y = k^*,\omega)$ after the wave packets collision is due to the fact that a bigger amount of energy is present at $k_y = k^* = 1.5$ due to the presence of nonlinear couplings which transfer the energy towards large wave numbers.

Before the collision (dot-solid red line), the energy is constrained in a relatively narrow band whose width is about few $\omega_0 \simeq 2\pi/T$. After the wave packets interaction (solid black line), the energy is instead significantly spread and the populated band width increases by a factor 5. The broadening of the dispersion relation suggests the presence of nonlinear turbulent couplings, whose explanation may be compatible with weak turbulence theory (nonlinear shift of the waves frequency) [60], either with strong turbulence theory (absence of dispersion relation). Moreover, in our simulation, the energy associated with $\omega \approx 0$ fluctuations significantly increases after the wave packets collision, as it can be appreciated in Figs. 3(c)–3(d) and in Fig. 4, thus suggesting the the production of quasistationary turbulent structures. Note that the energy distribution shown in the inset of Fig. 4 is peaked at $\omega \approx 0$ as also recovered in several solar wind observations [51–54].

IV. CONCLUSIONS

Here we described the interaction of two colliding Alfvénic wave packets by means of hybrid kinetic Vlasov-Maxwell simulations. We characterized the wave packets collision by analyzing the features which can be explained in terms of a linear modes approach and the signatures typical of a turbulent regime. Indeed, since the ratio of nonlinear time to overlap or collision time suggests the presence of a turbulent regime, it is interesting to study which linear mode features persist into a turbulent scenario and, on the other hand, which characteristics are definitively lost. A wavelike analysis, based on polarization and correlation, is still useful to characterize small-amplitude fluctuations that are found to be associated with KAW-like disturbances. However, signatures of a turbulent dynamics are also observed. In particular, (1) the energy in the ω-k plane is spread after the wave packets collision and the presence of dispersion relations is, in general, weakened and (2) the energy contained in the $\omega \approx 0$ fluctuations becomes dominant, thus suggesting the production of quasistationary current structures.

ACKNOWLEDGMENTS

Research is supported by NSF AGS-1460130 (SHINE), NASA grants NNX14AI63G (Heliophysics Grandchallenge Theory), the Solar Probe Plus science team (ISOIS/SWRI subcontract No. D99031L), and Agenzia Spaziale Italiana under the Contract No. ASI-INAF 2015-039-R.O. "Missione M4 di ESA: Partecipazione Italiana alla fase di assessment della missione THOR." Kinetic numerical simulations here discussed have been run on the Fermi parallel machine at Cineca, Italy, within the ISCRA-C Project No. IsC37-COLALFWP and on the Newton parallel machine at University of Calabria, Italy.

[1] U. Frisch, *Turbulence* (Cambridge University Press, Cambridge, 1995).
[2] W. M. Elsässer, Phys. Rev. **79**, 183 (1950).
[3] H. K. Moffatt, *Field Generation in Electrically Conducting Fluids* (Cambridge University Press, Cambridge, 1978).
[4] E. N. Parker, *Cosmical Magnetic Fields: Their Origin and Their Activity* (Oxford University Press, Oxford, 1979).
[5] M. Dobrowolny, A. Mangeney, and P. Veltri, Phys. Rev. Lett. **45**, 144 (1980).
[6] M. Velli, R. Grappin, and A. Mangeney, Phys. Rev. Lett **63**, 1807 (1989).
[7] W. H. Matthaeus, G. P. Zank, C. W. Smith, and S. Oughton, Phys. Rev. Lett. **82**, 3444 (1999).
[8] S. Galtier, S. V. Nazarenko, A. C. Newell, and A. Poucket, J. Plasma Phys. **63**, 447 (2000).
[9] A. Verdini, M. Velli, and E. Buchlin, Astrophys. J. Lett. **700**, L39 (2009).
[10] C. S. Ng and A. Bhattacharjee, Astrophys. J. **465**, 845 (1996).
[11] J. W. Belcher and L. Davis Jr., J. Geophys. Res. **76**, 3534 (1971).
[12] R. Bruno and V. Carbone, Living Rev. Solar Phys. **10**, 1 (2013).
[13] W. H. Matthaeus, G. P. Zank, S. Oughton, D. J. Mullan, and P. Dmitruk, Astrophys. J. Lett. **523**, L93 (1999).
[14] S. Tomczyk, S. W. McIntosh, S. L. Keil, P. G. Judge, T. Schad, D. H. Seeley, and J. Edmondson, Science **317**, 1192 (2007).
[15] S. Tomczyk and S. W. McIntosh, Astrophys. J. **697**, 1384 (2009).

[16] A. K. Srivastava, J. Shetye, K. Murawski, J. G. Doyle, M. Stangalini, E. Scullion, T. Ray, D. P. Wòjcik, and B. N. Dwivedi, Sci. Rep. **7**, 43147 (2017).

[17] R. Bruno, R. Bavassano, and U. Villante, J. Geophys. Res. **90**, 4373 (1985).

[18] D. J. McComas, L. Barraclough, H. O. Funsten, J. T. Gosling, E. Santiago-Muñoz, R. M. Skoug, B. E. Goldstein, M. Neugebauer, P. Riley, and A. Balogh, J. Geophys. Res. **105**, 10419 (2000).

[19] O. Alexandrova, V. Carbone, P. Veltri, and L. Sorriso-Valvo, Astrophys. J. **674**, 1153 (2008).

[20] F. Sahraoui, S. Galtier, and G. Belmont, J. Plasma Phys. **73**, 723 (2007).

[21] S. P. Gary, S. Saito, and Y. Narita, Astrophys. J. **716**, 1332 (2010).

[22] J. V. Hollweg, J. Geophys. Res. **104**, 14811 (1999).

[23] E. Marsch, Living Rev. Sol. Phys. **3**, 1 (2006).

[24] F. Valentini, P. Trávníček, F. Califano, P. Hellinger, and A. Mangeney, J. Comput. Phys. **225**, 753 (2007).

[25] F. Valentini, D. Perrone, and P. Veltri, Astrophys. J. **739**, 54 (2011).

[26] S. Servidio, F. Valentini, F. Califano, and P. Veltri, Phys. Rev. Lett. **108**, 045001 (2012).

[27] D. Perrone, F. Valentini, S. Servidio, S. Dalena, and P. Veltri, Astrophys. J. **762**, 99 (2013).

[28] F. Valentini, S. Servidio, D. Perrone, F. Califano, W. H. Matthaeus, and P. Veltri, Phys. Plasmas **21**, 082307 (2014).

[29] S. Servidio, F. Valentini, D. Perrone, A. Greco, F. Califano, W. H. Matthaeus, and P. Veltri, J. Plasma Phys. **81**, 325810107 (2015).

[30] J. He, C. Tu, E. Marsch, C. H. K. Chen, L. Wang, Z. Pei, L. Zhang, C. S. Salem, and S. D. Bale, Astrophys. J. Lett. **813**, L30 (2015).

[31] O. Pezzi, T. N. Parashar, S. Servidio, F. Valentini, C. V. Vásconez, Y. Yang, F. Malara, W. H. Matthaeus, and P. Veltri, Astrophys. J. **834**, 166 (2017).

[32] O. Pezzi, T. N. Parashar, S. Servidio, F. Valentini, C. V. Vásconez, Y. Yang, F. Malara, W. H. Matthaeus, and P. Veltri, J. Plasma Phys. **83**, 905830105 (2017).

[33] G. G. Howes and K. D. Nielson, Phys. Plasmas **20**, 072302 (2013).

[34] K. D. Nielson, G. G. Howes, and W. Dorland, Phys. Plasmas **20**, 072303 (2013).

[35] G. G. Howes, K. D. Nielson, D. J. Drake, J. W. R. Schroeder, F. Skiff, C. A. Kletzing, and T. A. Carter, Phys. Plasmas **20**, 072304 (2013).

[36] D. J. Drake, J. W. R. Schroeder, G. G. Howes, C. A. Kletzing, F. Skiff, T. A. Carter, and D. W. Auerbach, Phys. Plasmas **20**, 072901 (2013).

[37] D. J. Drake, G. G. Howes, J. R. Rhudy, S. K. Terry, T. A. Carter, C. A. Kletzing, J. W. R. Schroeder, and F. Skiff, Phys. Plasmas **23**, 022305 (2016).

[38] S. Sridhar and P. Goldreich, Astrophys. J. **432**, 612 (1994).

[39] S. Galtier, J. Plasma Phys. **72**, 721 (2006).

[40] P. H. Yoon, L. F. Ziebell, R. Gaelzer, and J. Pavan, Phys. Plasmas **19**, 102303 (2012).

[41] P. H. Yoon, Phys. Plasmas **22**, 082309 (2015).

[42] P. H. Yoon, Phys. Plasmas **22**, 082310 (2015).

[43] A. Hasegawa and L. Chen, Phys. Fluids **19**, 1924 (1976).

[44] E. A. Frieman and L. Chen, Phys. Fluids **25**, 502 (1982).

[45] L. Rudakov, M. Mithaiwala, G. Ganguli, and C. Crabtree, Phys. Plasmas **18**, 012307 (2011).

[46] R. Meyrand, S. Galtier, and K. H. Kiyani, Phys. Rev. Lett. **116**, 105002 (2016).

[47] P. Goldreich and S. Sridhar, Astrophys. J. **438**, 763 (1995).

[48] A. Barnes, J. Geophys. Res. **84**, 4459 (1979).

[49] W. H. Matthaeus, S. Oughton, K. T. Osman, S. Servidio, M. Wan, S. P. Gary, M. A. Shay, F. Valentini, V. Roytershteyn, H. Karimabadi, and S. C. Chapman, Astrophys. J. **790**, 155 (2014).

[50] W. H. Matthaeus, M. Wan, S. Servidio, A. Greco, K. T. Osman, S. Oughton, and P. Dmitruk, Phil. Trans. R. Soc. London **373**, 20140154 (2015).

[51] Y. Narita, S. P. Gary, S. Saito, K. H. Glassmeier, and U. Motschmann, Geophys. Res. Lett. **38**, L05101 (2011).

[52] O. W. Roberts and X. Li, Astrophys. J. **802**, 1 (2015).

[53] O. W. Roberts, X. Li, and L. Jeska, Astrophys. J. **802**, 2 (2015).

[54] C. Perschke, Y. Narita, U. Motschmann, and K. H. Glassmeier, Phys. Rev. Lett. **116**, 125101 (2016).

[55] H. Karimabadi, V. Roytershteyn, M. Wan, W. H. Matthaeus, W. Daughton, P. Wu, M. Shay, B. Loring, J. Borovksy, E. Leonardis, S. C. Chapman, and T. K. Nakamura, Phys. Plasmas **20**, 012303 (2013).

[56] C. Vásconez, F. Valentini, E. Camporeale, and P. Veltri, Phys. Plasmas **21**, 112107 (2014).

[57] See Supplemental Material at http://link.aps.org/supplemental/10.1103/PhysRevE.96.023201 for the temporal evolution of $j_z(x,y,t)$.

[58] C. Vásconez, F. Pucci, F. Valentini, S. Servidio, W. Matthaeus, and F. Malara, Astrophys. J. **815**, 7 (2015).

[59] F. Pucci, C. L. Vásconez, O. Pezzi, S. Servidio, F. Valentini, W. H. Matthaeus, and F. Malara, J. Geophys. Res. **121**, 1024 (2016).

[60] J. D. Crawford, S. Johnston, A. N. Kaufman, and C. Oberman, Phys. Fluids **29**, 3219 (1986).